

GERMANIUM SILICON TIN OXIDE THIN FILMS FOR
UNCOOLED INFRARED DETECTORS

by

JAIME DAMIANY CARDONA

A THESIS

Submitted in partial fulfillment of the requirement
for the degree of Master of Science in the
Applied Optics Graduate Program
of Delaware State University

DOVER, DELAWARE
AUGUST 2019

This thesis is approved by the following members of the Final Oral Review Committee:

Dr. Mukti Rana, Committee Chairperson, Division of Physical and Computational Sciences,
Delaware State University

Dr. Mohammed Khan, Committee Member, Division of Physical and Computational Sciences,
Delaware State University

Dr. Qi Lu, Committee Member, Division of Physical and Computational Sciences, Delaware
State University

Dr. Bizuneh Workie, External Committee Member, Department of Chemistry, Delaware State
University

DEDICATION

To NDB who shaped my past, present, and sent me forth towards a future.

ACKNOWLEDGEMENTS

I would like to thank Dr. Mukti Rana for taking me into his group late in the Spring last year (2018), and teaching me about the development and background of semiconductor devices. Next I would like to thank the members of my committee, Dr. Mohammed Khan, Dr. Qi Lu, and Dr. Bizuneh Workie for agreeing to be in my committee, and taking time out of their day to review my work.

I would like to thank my group members Nick Calvano and Andrew Voshell for their assistance and guidance as after I joined the group. I would like to thank Rishi Gundakaram and Megan Powers, it was with their assistance that I developed most of the testing process used in this work.

Germanium Silicon Tin Oxide Thin Films for Uncooled Infrared Detectors

Jaime D. Cardona

Faculty Advisor: Dr. Mukti Rana

Abstract

Microbolometer is a class of infrared detector whose resistance changes when the temperature changes. In this work, we deposited and characterized Germanium Silicon Oxide thin films mixed with Tin (Ge-Si-Sn-O) for uncooled infrared detection. Ge-Sn-O was deposited by co-sputtering of Sn and Ge-Si targets in an Ar+O environment using a radio frequency (RF) and direct current (DC) sputtering system. The electrical and optical properties of the thin films were tested to verify whether Ge-Si-Sn-O could be used as a sensing material in a microbolometer. From this testing, it was shown that with the an atomic composition consisting of $\text{Ge}_{0.36}\text{Si}_{0.04}\text{Sn}_{0.11}\text{O}_{0.43}$ the Ge-Si-Sn-O alloy could have a temperature coefficient of resistance (TCR) greater than -3.5 %/K, optical band gap of around 1 eV, and noise value of $300 \mu\text{V}/\sqrt{\text{Hz}}$ at 10Hz. With these values, besides the slightly high noise value, it has been determined that Ge-Si-Sn-O alloy is a viable candidate for use in microbolometer development.

Table of Contents

List of Figures.....	vii
List of Tables	viii
List of Abbreviations.....	ix
Chapter 1: INTRODUCTION	1
1.1 Infrared Radiation	1
1.1.1 Use of Infrared Radiation	1
1.2 Thermographic Detector	2
1.3 Microbolometer	3
1.3.1 Spectral Response	3
1.3.2 Thermal Conductivity.....	4
1.3.2.1 Temperature Coefficient of Resistance	5
1.3.3 Responsivity.....	5
1.3.4 Detectivity.....	6
1.3.5 Noise Equivalent Power	6
1.3.6 Noise Equivalent Temperature Difference	6
1.3.7 Sources of Noise	7
1.4 Synopsis	9
Chapter 2: FABRICATION AND CHARACTERIZATION OF $\text{Ge}_x\text{Si}_y\text{Sn}_z\text{O}_{1-x-y-z}$ THIN FILMS	10
2.1 Thin Films Development.....	10
2.1.1 Materials Used in Sensing Layer Thin Films	10
2.1.2 Sputtering.....	11
2.2 Thin Film Characterization Process.....	14
Chapter 3: RESULTS OF $\text{Ge}_x\text{Si}_y\text{Sn}_z\text{O}_{1-x-y-z}$ THIN FILMS	23
Chapter 4: DISCUSSION AND CONCLUSION	38
Appendix A.....	40
Appendix B	41

References42

LIST OF FIGURES

Fig. 1.1 Simplified microblometer cross section	3
Figure 2.1 Sputtering	11
Figure 2.2 Ge-Si target	12
Figure 2.3 Inside the Lesker sputtering chamber	13
Figure 2.4 Film thickness measurement	15
Figure 2.5 EDS plot	16
Figure 2.6 EBSD figure	17
Figure 2.7 Four-point probe	20
Figure 2.8 Transmittance and Reflectance measurement setup	21
Figure 2.9 Noise measurement setup	22
Figure 3.1 Plot of $\ln(\rho)$ vs $1/k_B T$ for $\text{Ge}_{0.36}\text{Si}_{0.04}\text{Sn}_{0.11}\text{O}_{0.43}$	24
Figure 3.2 Variation of TCR with Oxygen concentration	25
Figure 3.3 Variation of TCR with Tin Concentration	26
Figure 3.4 Plot of $\ln(\rho)$ vs $1/kT$ plot for $\text{Ge}_{0.41}\text{Si}_{0.01}\text{Sn}_{0.09}\text{O}_{0.42}$	27
Figure 3.5 Transmittance of four different GeSiSnO thin films	29
Figure 3.6 Reflectance of four different GeSiSnO thin films	30
Figure 3.7 Absorption of four different GeSiSnO thin films	31
Figure 3.8 Optical band gap plot for GeSiSnO	32
Figure 3.9 Variation of Optical band gap and Oxygen concentration	33
Figure 3.10 Variation of Optical band gap and Tin concentration	34
Appendix A Patent Approval Letter	39

LIST OF TABLES

Table 3.1	36
------------------------	-----------

LIST OF ABBREVIATIONS

IR	Infrared
NIR	Near infrared
SWIR	Short wavelength infrared
MWIR	Mid wavelength infrared
LWIR	Long wavelength infrared
FWIR	Far wavelength infrared
TCR	Temperature coefficient of resistance
NEP	Noise equivalent power
NETD	Noise equivalent temperature dependence
RF	Radio frequency
DC	Direct current
Ge	Germanium
Si	Silicon
Sn	Tin
O	Oxygen
EDS	Electron dispersive x-ray spectroscopy
EBSD	Electron backscatter diffraction

CHAPTER 1: INTRODUCTION

1.1 Infrared Radiation

Infrared (IR) radiation is the part of the electromagnetic spectrum ranging from 0.75 to 1,000 μm . This range can be further divided into multiple smaller ranges known as: near IR (NIR) from 0.75 to 1.4 μm , short wavelength IR (SWIR) from 1.4 to 3 μm , mid wavelength IR (MWIR) from 3 to 8 μm , long wavelength IR (LWIR) from 8 to 15 μm , and far wavelength IR (FWIR) from 15 to 1,000 μm . All objects whose temperature is greater than absolute zero radiate IR radiation according to Planck's law.

$$B_{\lambda}(\lambda, T) = \frac{2hc^2}{\lambda^5} \frac{1}{e^{\frac{hc}{\lambda k_B T}} - 1} \quad (1.1)$$

Where, B is the spectral radiance of a body at absolute temperature T , h is Planck's constant, k_B is Boltzmann's constant, and c is the speed of light [1].

1.1.1 *Use of Infrared Radiation*

IR radiation is used for various applications. The differences in temperature can be detected as different IR wavelengths, and those differences can then be used to develop images. The use of developing images based on temperature differences is defined as infrared thermography, and the detectors used for this purpose are known as thermal detectors. Usually these thermographic cameras/detectors operate in the LWIR, and allow for imaging in areas that are not well lit. As such they are useful for search and rescue as well as surveillance; making this technology pivotal for military purposes. Outside of military use, there is IR astronomy where specially equipped telescopes are used to spot objects in space that are hidden behind dust clouds or are red shifted. Recently thermal imaging cameras have started to see use in camera based autonomous driving systems.

1.2 Thermographic Detector

There are two main types of thermographic detector: cooled and uncooled. Cooled detectors have to be cryogenically cooled in order to function, usually to around 100 K. Cooled detectors are generally expensive, bulky, and require time to cool down before they can be used. Uncooled detectors are operational at temperature close to ambient room temp 295 K. These uncooled detectors are cheaper to produce and operate as they do not require the cooling equipment, and as such can be scaled down in size so that they are portable. The obvious tradeoff for these advantages is that the uncooled detectors are not as precise as cooled detectors, at least not with the current technology. Both cooled and uncooled detectors rely on semiconducting materials and their interaction with heating caused by IR. Depending on the type of detector and material used, the change in temperature will cause a change in certain electrical properties such as the resistance, capacitance, voltage, or inductance of the semiconducting material. Heating induced in the sensing materials due to IR absorption in them and triggers the electrical properties to be changed. Hence, the ability of the sensing material to absorb IR radiation is one of the most important properties that need to be determined for cooled or uncooled IR detection applications. For this work, the type of detector explored is the uncooled detector known as the microbolometer.

1.3 Microbolometer

Microbolometer is a type of uncooled IR detector whose resistance changes with temperature. Typical cross sectional area of a microbolometer is shown in Figure 1.1.

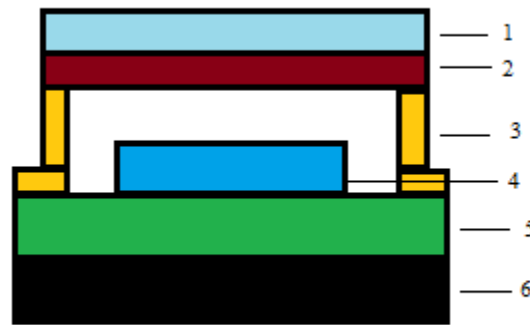


Figure 1.1 Simplified microbolometer cross-section

The six layers shown in Fig. 1 correspond in descending order from one to six: (1) absorbing layer, (2) semiconductor sensing layer, (3) electrode arms, (4) reflector inside a cavity, (5) insulation layer, and (6) substrate/readout circuit. The figures of merits for a microbolometer include spectral response, thermal conductivity, responsivity, detectivity, noise-equivalent power, and noise-equivalent temperature difference.

1.3.1 Spectral Response

The spectral response describes the sensitivity of the detector to radiation of different wavelengths. If for example at a low wavelength the detector has little to no response then the detector would not be optimal for use at that wavelength. For a thermal detector which responds to radiant power, it would have a spectral response due to unit radiant power per unit wavelength.

1.3.2 Thermal Conductivity

The performance of a thermal detector depends upon the thermal capacity C_{th} , the rate at which thermal energy is lost through the thermal conductance of the structure, G_{th} , and the radiative thermal conductance, G_{rad} . The radiative thermal conductance for a gray body, assuming the emissivity is equal to the absorptivity, is given by equation:

$$G_{rad} = 4\eta\sigma AT^3 \quad (1.2)$$

Where, η is optical absorption efficiency of the detector, σ is the Stefan-Boltzmann constant, A is the surface area, and T is the absolute temperature. The conductive/convective loss is neglected since the detector is typically operated in vacuum. The temperature change due to a sinusoidal modulated photon flux is given by [2,3]:

$$\Delta T = \frac{\eta\Phi}{G_{eff}(1 + \omega^2\tau_{th}^2)^{1/2}} \quad (1.3)$$

Where, Φ is the radiant energy flux, ω is the angular modulation frequency of the incident radiation, and τ_{th} the thermal time constant.

τ_{th} is defined as

$$\tau_{th} = \frac{G_{th}}{C_{th}} \quad (1.4)$$

The effective thermal conductance, G_{eff} , is obtained through a heat balance equation and is given by:

$$G_{eff} = G_{th} + G_{rad} \pm \alpha P_{bias} \quad (1.5)$$

Where, α is the TCR of the thermometer and P_{bias} is the power dissipated in the bias of the detector.

The sign of the power bias term depends upon the type of bias. The “+” sign corresponds to the voltage bias case while the “-” sign corresponds to the current bias case. For the case of a

semiconductor microbolometer, the TCR is negative, which means that the power dissipated in the detector effectively increases G_{eff} .

1.3.2.1 Temperature Coefficient of Resistance (TCR)

TCR exhibits how the resistance of the sensing material responds to a change in temperature and is expressed as:

$$\alpha = \frac{1}{R} \frac{dR}{dT} = -\frac{E_a}{k_B T^2} \quad (1.6)$$

Where, E_a is the activation energy given in eV.

TCR is a material property, so the higher the value; the better it is for IR uncooled detection.

1.3.3 Responsivity

Responsivity is the measure of the input to output gain of the detector. A detector can give both current responsivity and voltage responsivity. Voltage responsivity R_v is defined as the detector output voltage with respect to the detector input power.

$$R_v = \frac{\eta \alpha R I_b}{G_{th}(1 + \omega^2 \tau^2)^{1/2}} \quad (1.7)$$

Where, I_b is the bias current, ω is the angular frequency, and τ is the time constant of the device.

The first three terms of the numerator in the right-hand side of equation (1.7) depend on material properties of the microbolometer. Voltage responsivity is expressed in V/W while current responsivity is expressed in A/W. The voltage responsivity of the bolometer is increased by decreasing the thermal conductance of the structure. The thermal time constant of the microbolometer is in the millisecond range as it involves the thermal mass of the sensing layer which needs to heat up for change in resistance because of IR radiation.

1.3.4 Detectivity

Detectivity, D^* , is the area normalized signal to noise ratio. It has the unit of $\text{cmHz}^{1/2}/\text{W}$. The detectivity is expressed by:

$$D^* = \frac{R_v \sqrt{A_d \Delta f}}{\Delta v_n} \quad (1.8)$$

where Δv_n is the total noise voltage observed in the electrical bandwidth Δf and is the sum of noises from the sensing element of the microbolometer – Johnson noise, $1/f$ -noise, generation and recombination (g-r) noise. Higher responsivity represents higher detectivity, and a high detectivity and TCR mean a better performing microbolometer[4].

1.3.5 Noise Equivalent Power

Noise equivalent power, which is in Watts, is the input signal power that results in a signal-to-noise ratio of one in one hertz output bandwidth [5]. NEP is related to detectivity by:

$$NEP = \frac{(A_d * \Delta f)^{1/2}}{D^*} \quad (1.9)$$

Where A_d is the area of the detector element and Δf is the bandwidth of the noise.

1.3.6 Noise Equivalent Temperature Difference

NETD is defined as the temperature difference between a test target and the background that produces a signal equivalent to the (temporal) noise [6-8]. NETD can be mathematically expressed as:

$$NETD = \frac{4F^2}{\tau_o D^* \sqrt{A_d} (\Delta P / \Delta T)_{\lambda_1 - \lambda_2}} \quad (1.10)$$

Where, F is the f-number of the optics, τ_o is the transmittance of the optics,

$(\Delta P / \Delta T)_{\lambda_1 - \lambda_2}$ is the derivative with respect to temperature of the power radiated by a blackbody at room temperature within the spectral range between λ_1 and λ_2 .

1.3.7 Sources of Noise

As mentioned in section (1.3.4), there is five sources of noise from the sensing element of the microbolometer to consider, as well as background and temperature fluctuation noise to consider when determining the viability of the detector as the limiting factor for all the figures of merit is the noise [9]. Of the five sources inherent to the sensing layer, $1/f$ -noise is the most dominant source of noise [10]. For a physical sample the $1/f$ -noise can be expressed as [10]:

$$V_{1/f} = KV_B \sqrt{\frac{\rho}{WLtf}} \quad (1.11)$$

Where, K is a constant that depends on the material, V_B is the bias voltage, ρ is the resistivity, f is the electrical frequency, and W , L , t are the width, length, and thickness of the active part of the microbolometer.

From (1.11) it is shown that $1/f$ -noise is dependent on the physical characteristics of the sensing layer of the microbolometer. $1/f$ -noise exists in the low frequency and disappears in white thermal noise that is always present. The causes of $1/f$ -noise are still up for debate.

Johnson noise is caused by random motion in charge carriers in any resistive element with temperature above absolute zero. Meaning all circuits are subject to Johnson noise, Johnson noise can be represented as:

$$V_j = \sqrt{4k_B TR\Delta f} \quad (1.12)$$

Where Δf is the frequency bandwidth over which the noise is measured. Johnson noise is seen in the high frequency range.

Temperature fluctuation noise is caused by the exchange of energy between the device and its substrate, through conductance. Temperature fluctuation noise is given by [11]:

$$V_{TF} = \frac{2I_B R \alpha T}{\sqrt{G_{th}(1 + \omega^2 \tau_{th}^2)}} \sqrt{\Delta f k_B} \quad (1.13)$$

Where, ω is the modular frequency of the incident IR radiation.

Background noise is the noise from random fluctuations between the detector and a nearby blackbody. The background noise can be expressed as [11]:

$$V_{BG} = \frac{I_B R \alpha}{G_{th} \sqrt{(1 + \omega^2 \tau_{th}^2)}} \sqrt{8 A_d \sigma \eta \Delta f k_B (T^5 + T_B^5)} \quad (1.14)$$

Where, T_B is the temperature of the blackbody.

Generation and recombination noise (V_{g-r}) is caused by the fluctuations of charge carriers due to generation recombination centers. This type of noise is a function of temperature as well the biasing conditions.

The total noise that you could see in a microbolometer is the summation of all the previous noises listed.

$$V_T = \sqrt{V_{1/f} + V_j + V_{TF} + V_{BG} + V_{g-r}} \quad (1.15)$$

It is worth noting that depending on the range of frequencies certain types of noise will dominate so 1.14 can be simplified to something like:

$$V_T = \sqrt{V_{1/f} + V_j + V_{TF}} \quad (1.16)$$

Where *1/f-noise* dominates the low frequency range and the Johnson and thermal fluctuation noise dominate in the mid to high frequencies.

1.4 Synopsis

The focus of this chapter was on infrared detectors, microbolometers in particular, and their defining characteristics were discussed. The focus of this project is to investigate a new alloy to be used as the sensing layer of a microbolometer, $\text{Ge}_x\text{Si}_y\text{Sn}_z\text{O}_{1-x-y-z}$. For this purpose, the new

alloy will be investigated from development to characterization. $\text{Ge}_x\text{Si}_{1-x}\text{O}_y$ has been shown to have a high a temperature coefficient of resistance, and has been tested for us in microbolometer technology [12]. The addition of tin was made in order to increase the amount of IR radiation absorption. With this in mind, the hypothesis is that our new material will surpass the performance of two most commonly used microbolometer materials – vanadium oxide (VOx) and amorphous silicon (a-Si). Vanadium oxide and a-Si have a TCR of about -3 %/K and -2 %/K respectively [13, 14]. The motivation of this work is to develop a new microbolometer material which has a TCR greater than that of VOx and a-Si, as well as having an optical band gap small enough so that the film is useable for the range of 2 to 5 μm and 8 to 12 μm .

CHAPTER 2: FABRICATION AND CHARACTERIZATION OF $\text{Ge}_x\text{Si}_y\text{Sn}_z\text{O}_{1-x-y-z}$ THIN FILMS

2.1 Thin Films Development

2.1.1 *Materials Used in Sensing Layer Thin Films*

The sensing for a microbolometer could in theory be made up of any element/alloy whose resistance has temperature dependence value. In practice, the sensing viability of element/alloy depends on four conditions being met:

- 1.) High IR radiation absorption
- 2.) High TCR, so that small changes in temperature will result in a greater image contrast
- 3.) A resistivity that is not too large, otherwise the microbolometer interface circuit cannot be integrated with the sensing layer.
- 4.) Low $1/f$ -noise

Also, in order to be compatible with the complementary metal-oxide-semiconductor CMOS circuit development that is used in micromachining a microbolometer a conventional semiconductor is preferred.

The film can be deposited by physical vapor deposition process such as sputtering or other processes such as evaporation, chemical vapor deposition processes among others. For our work we used the sputtering process to deposit our films as this is relatively simple and inexpensive.

2.1.2 *Sputtering*

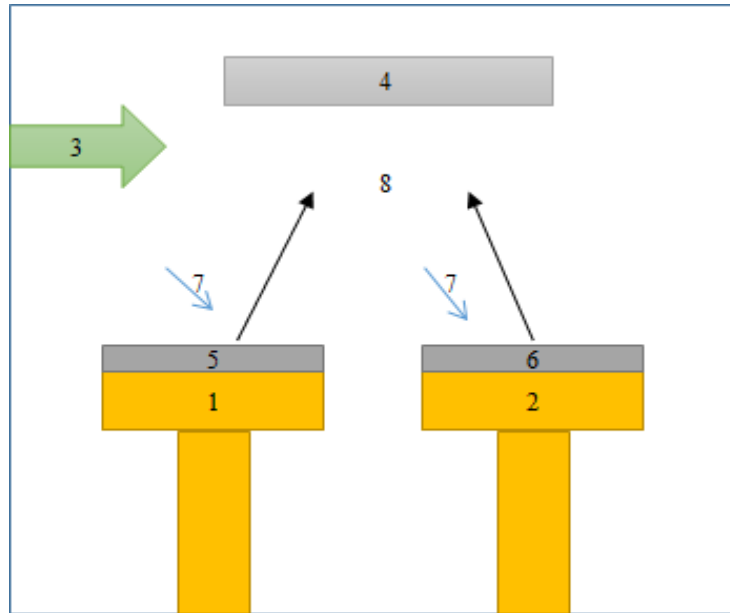


Fig 2.1 Sputtering: (1) RF gun, (2) DC gun, (3) Ar + O₂ gas, (4) substrate holder, (5) Ge-Si target, (6) Sn target, (7) Ionized Ar gas, (8) Particles from the targets

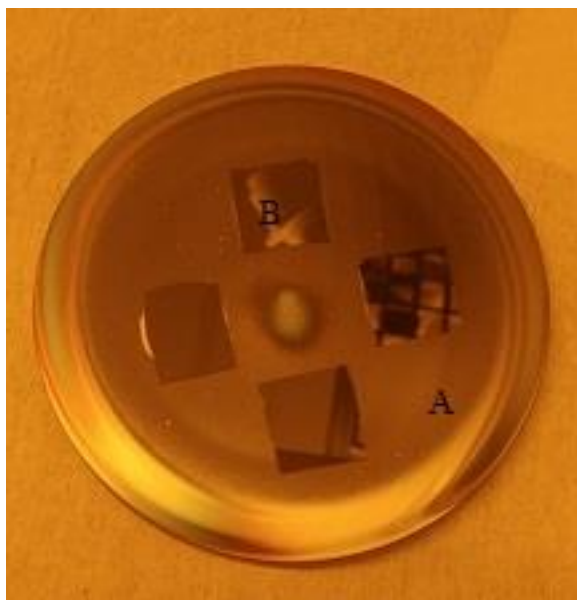


Fig 2.2 Ge-Si target: (A) Germanium target, (B) Silicon pieces. Silicon pieces are cleaned using hydrofluoric acid (HF) etching in order to remove any oxide layers.



Fig 2.3 Inside the Lesker sputtering chamber. Ge-Si target mounted on RF gun in the front, Sn mounted on DC gun in the back, and the column on top is where the substrate is placed. Before sputtering begins targets are cleaned through the use of plasma. This same plasma is what is used to sputter the targets. In the case of cleaning the target the shutters are kept down.

The development and testing of the GeSiSnO thin film is done in a three-step process. The first step is to make the film through radio frequency (RF) and direct current (DC) magnetron sputtering in a custom build Kurt J Lesker sputtering system. Sputter deposition is a form of physical vapor deposition where the ionized Argon gas is used to bombard a Ge-Si target and a tin target, the targets then eject their materials onto a substrate placed above them. The Ge-Si compound target is a combination of a pure Ge target that then has pure squares of Si silver attached on top of it (Ge target). The area occupied by Si is set to 15 % of the total area of the Ge target, as this was seen to be the optimal amount for Ge-Si-O alloys Iborra et al [15]. The chamber was evacuated to 1×10^{-7} Torr and then was raised to 3 mTorr during the deposition stage. The RF and DC power was set to 180 W and 30 W respectively. The RF gun was used to sputter the Ge-Si material while the DC power was used to sputter the Sn.

The film was deposited onto three types of substrates: glass, Al_2O_3 (sapphire), and Ge. The film deposited on glass, is used for testing the electrical properties of the film whereas the sapphire and Ge substrate are used to test the optical properties of the film.

2.2 Thin Films Characterization Process

Before checking the electrical and optical properties of the film, the thickness of the film was measured. Film thickness was determined through the use of Bruker DektakXT profilometer. The profilometer would average the thickness from five separate runs. Fig 2.4 shows the thickness was measured to be 47322.29 Å.

Another important step taken before testing the electrical and optical properties is to determine the atomic composition and structure of the sample. This is done by using energy dispersive x-ray spectroscopy (EDS) and electron backscatter diffraction (EBSD). By performing

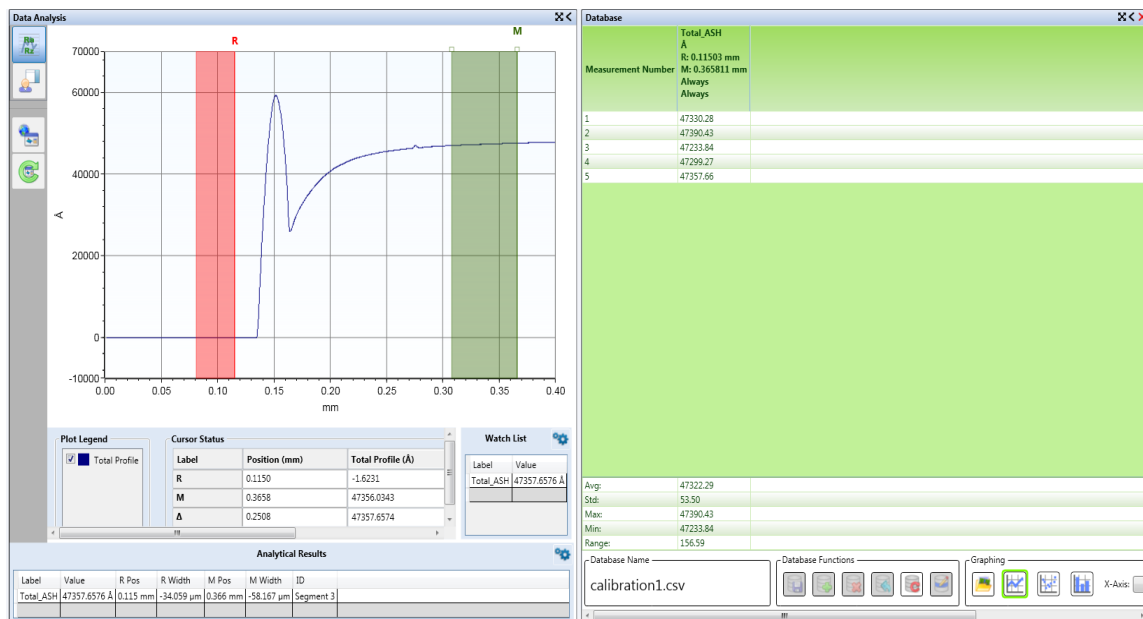


Fig 2.4 Film thickness measurement

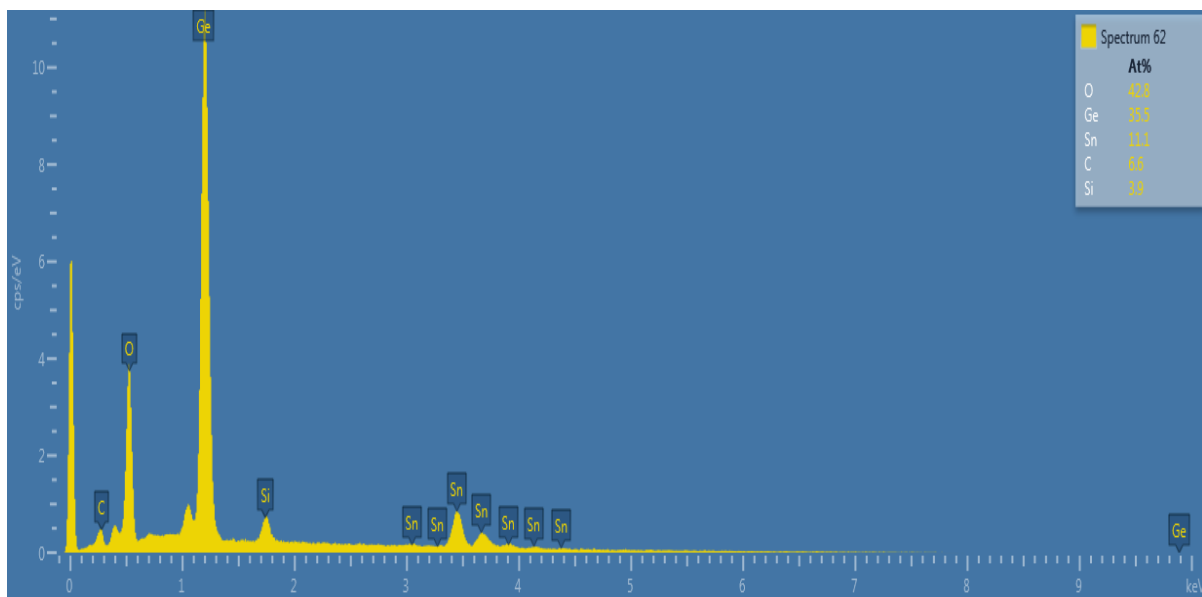


Fig 2.5 EDS figure produced by the Aztec software suite of a GeSiSnO thin film, shown is

the results for $\text{Ge}_{0.36}\text{Si}_{0.04}\text{Sn}_{0.11}\text{O}_{0.43}$.

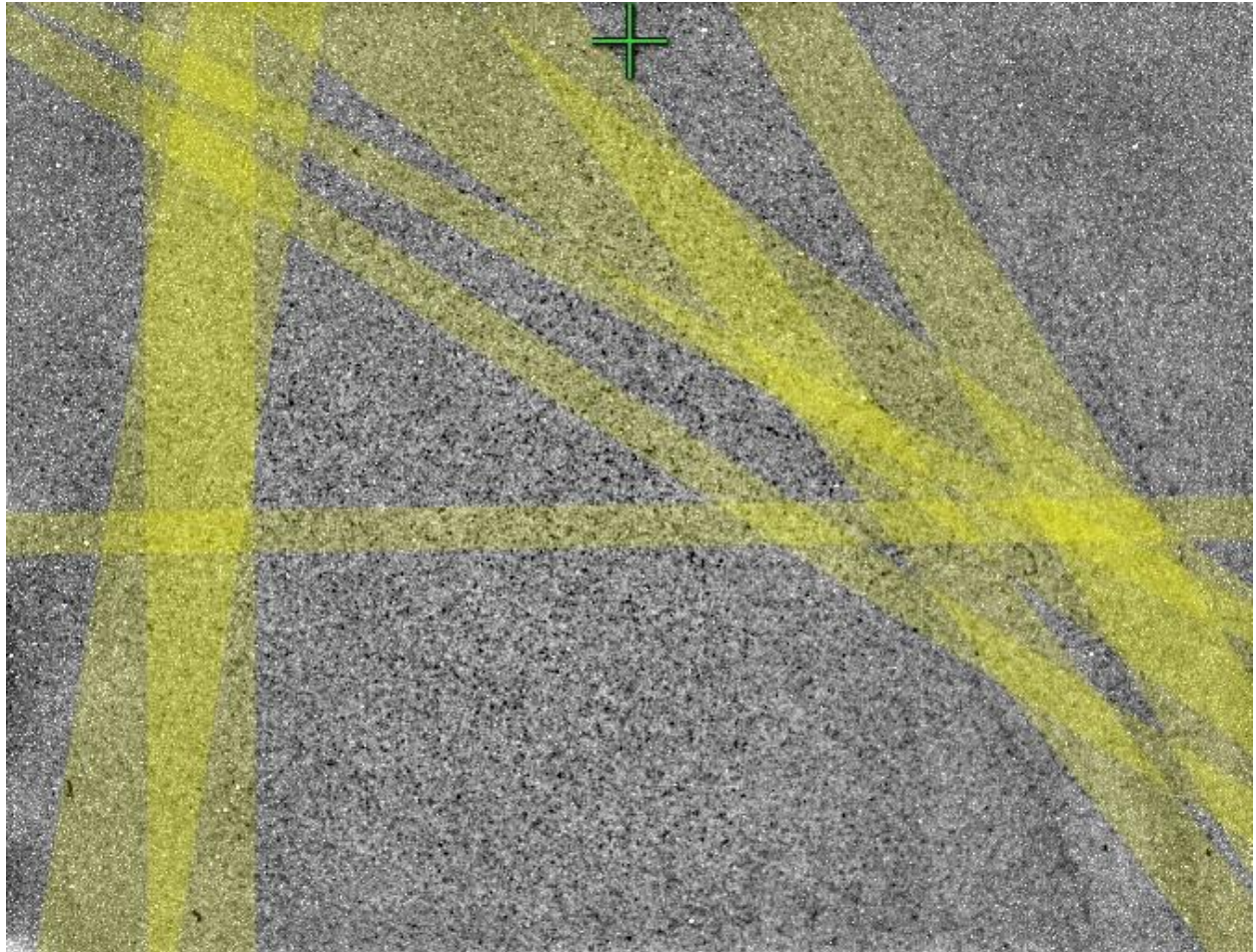


Fig 2.6 EBSD spectra for GeSiSnO thin film to determine the crystal structure

EDS/EBSD in a FEI Quanta FEG 250 SEM on the sample, the composition/crystalline structure of the sample is determined using the Aztec software package. EDS/EBSD is accomplished through the use of an electron beam hitting the sample. In EDS an electron at a lower shell will be displaced by the beam and leave a hole that is replaced by a higher shell electron. This movement produces a x-ray that is characteristic to a specific element. In EBSD the sample is placed at 70 degrees away from the beam. The electrons then will backscatter off the sample. Electrons that are backscattered near the Bragg angle will form Kikuchi bands, the yellow lines in Fig 2.6. These bands can be indexed using the Miller indices. If the sample has a well-defined crystal structure the yellow lines will form a pattern. In Fig 2.6 there is no pattern meaning the sample has no discernable crystal structure and is amorphous in nature. For the system that was used there would be a carbon peak due to carbon noise and not the sample itself. This can be seen in Fig 2.5. In Fig 2.5 there are also unidentified peaks which correspond to the substrate. In the case of these small peaks the beam penetrated through the sample and into the glass substrate. There was not a significant amount of substrate material which is why the peaks are unlabeled.

Next the resistivities of the samples were calculated through the use of a four point-probe. Using a Jandel 3000 Test Unit, four point-probe, and micromanipulator stage the sheet resistance of the film was found; as can be seen in Fig 2.7. The temperature of the sample was varied from 17 to 37 degrees Celsius and the sheet resistance was measured at the different temperatures. Using (2.1) resistivity (ρ) can be calculated.

$$\rho = R_{sheet} * t \quad (2.1)$$

Where R_{sheet} is the sheet resistance and t is thickness of the sample.

For the optical measurements we used the setup depicted in Fig 2.8. By using a silicon carbide light source and monochromator different wavelengths of light can be passed through the

sample, this enables the testing of the transmittance and reflection. First the measurement is made for light passing through air. This becomes the total amount of light; from there transmittance and reflectance are determined as a percentage of that total light. Depending on the wavelengths this is where the other substrates come in. Glass for 1 to 3 μm , sapphire for 2 to 5 μm , and germanium for 6-10 μm . The reason substrates are used is that they have a high or relatively high transmittance in those wavelength regions [16-18]. As mentioned before transmittance and reflectance are a percentage of the total light therefore whatever light is not transmitted or reflected should be the amount of light that was absorbed. The absorption can then be calculated by using (2.2)

$$1 = T + R + A \quad (2.2)$$

Once the results are collected the composition of the film is altered slightly and then measured again. In this way we are able to determine what atomic composition has the highest TCR while maintaining an optimal optical band gap.

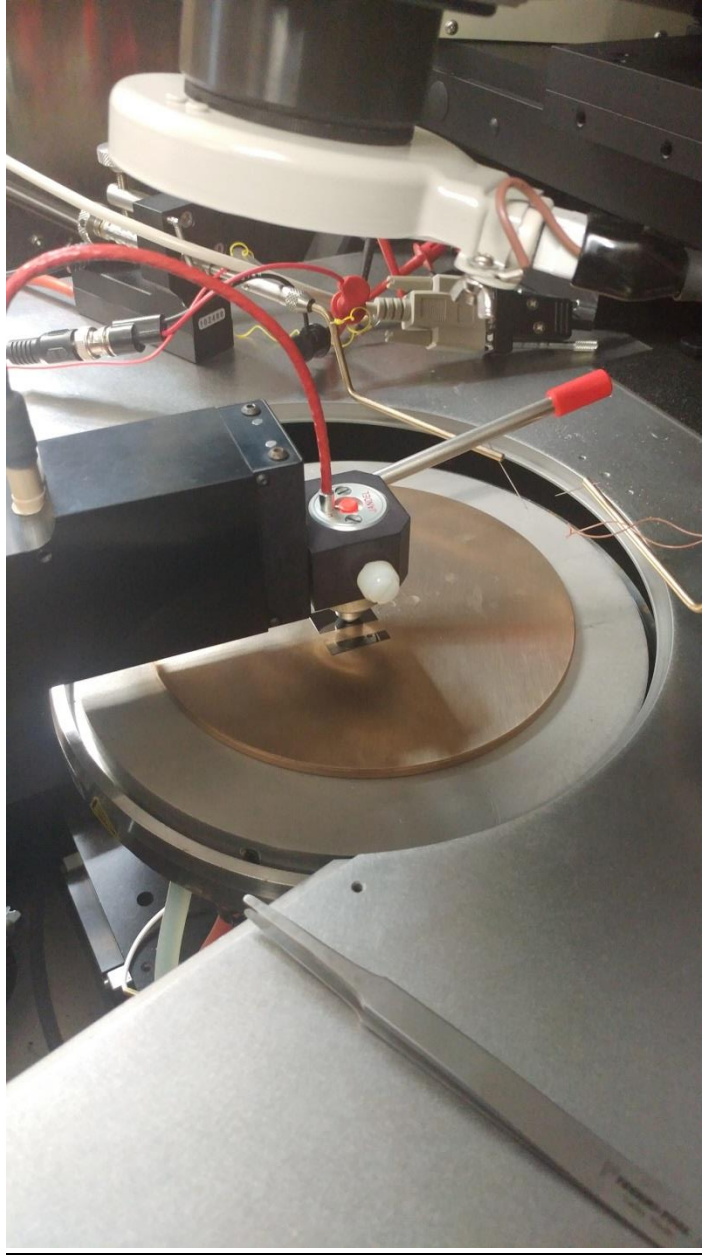


Fig 2.7 Four-point probe on micromanipulator stage to determine R_{sheet}

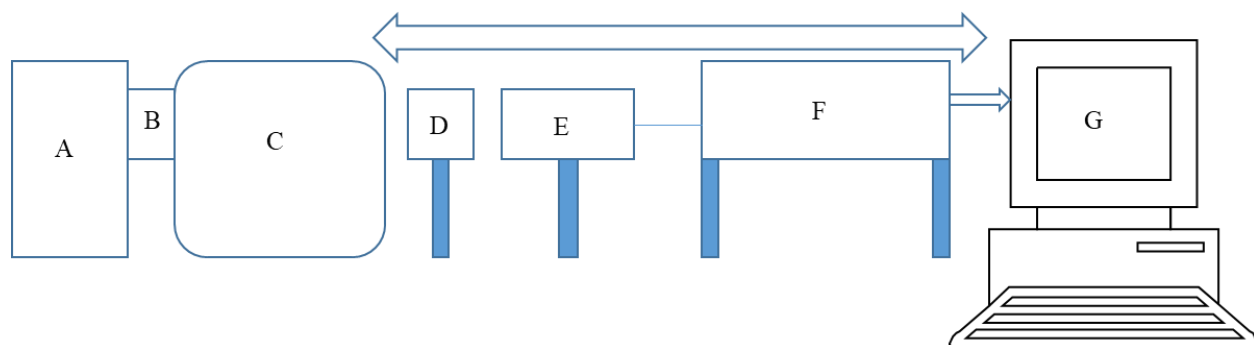


Fig 2.8 Transmittance and Reflectance measurement setup

A.) Blackbody (Silicon Carbide bar) Light Source

B.) Newport Optical Chopper

C.) Monochromator

D.) Thin Film

E.) Newport Pyroelectric Detector

F.) SRS SR 810 DSP Lock-In Amplifier

G.) Computer

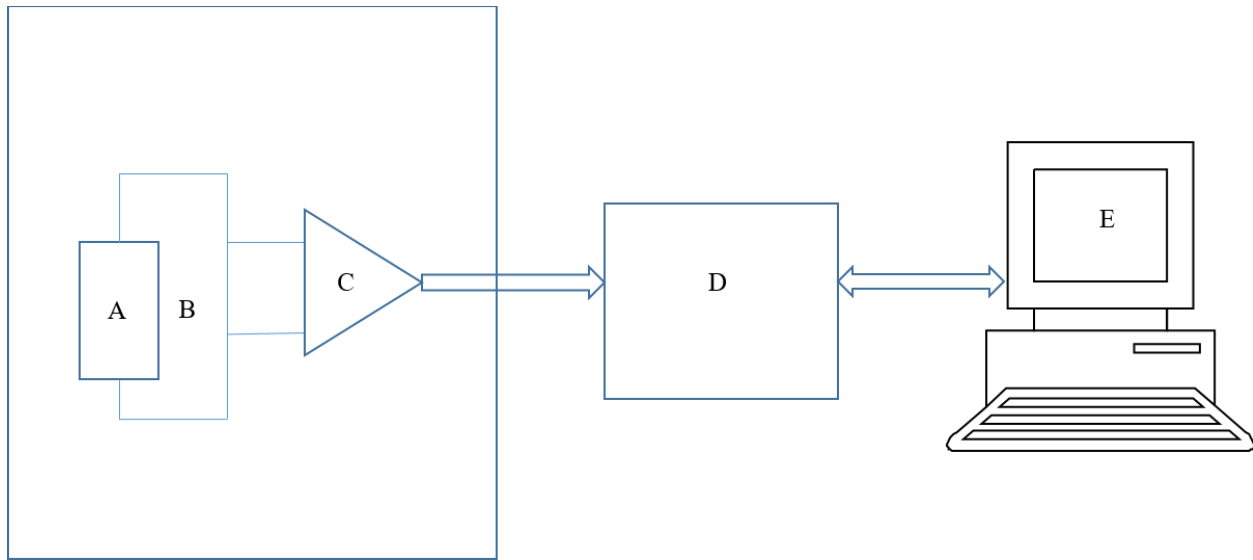


Fig 2.9 Noise measurement setup

A.) Thin Film Sample

B.) Current Circuit

C.) Low Noise Pre-Amplifier SRS 560

D.) Keysight Signal Analyzer

E.) Computer

CHAPTER 3: RESULTS OF $\text{Ge}_x\text{Si}_y\text{Sn}_z\text{O}_{1-x-y-z}$ THIN FILMS

Multiple sets of samples were developed mainly through the increase/decrease in oxygen and tin concentration. Activation energy is related to resistance by:

$$R(T) = R_o e^{\frac{E_a}{k_B T}} \quad (3.1)$$

Where $R(T)$ is the resistance at temperature T , R_o is the pre-exponential factor, and E_a is the activation energy.

An Arrhenius plot of $\ln(\rho)$ vs $1/kT$ was developed and a straight line plot was calculated using a line of best fit for each of the samples. Fig 3.1 is the $\ln(\rho)$ vs $1/kT$ plot for sample $\text{Ge}_{0.36}\text{Si}_{0.04}\text{Sn}_{0.11}\text{O}_{0.43}$. From this plot, we can see that it is not exactly linear meaning that R_o has weaker temperature dependence than if it had been completely linear. Fig 3.2 and 3.3 show how TCR vary with oxygen and tin concentration. The trends of these plots show that a high oxygen concentration and a lower tin concentration will lead to a higher TCR value. There is an outlier when the oxygen concentration is higher than 40% and the tin concentration is lower than 10%. In Fig 3.4 it is shown that $\text{Ge}_{0.41}\text{Si}_{0.01}\text{Sn}_{0.09}\text{O}_{0.42}$ is even less linear in nature than what can be seen in Fig 3.1. This is caused by switch in the usual semiconductor behavior. When a semiconductor is heated the resistance is supposed to fall, but for this particular sample there was a temperature region in which the resistance increased. Eventually the film returned to having the usual semiconductor behavior. The linearity and slope of the $\ln(\rho)$ vs $1/kT$ plots are determined by the activation energy value of the thin film sample. If the plot is not linear and has a small slope this equates to the film having low activation energy, and this means that the film will have

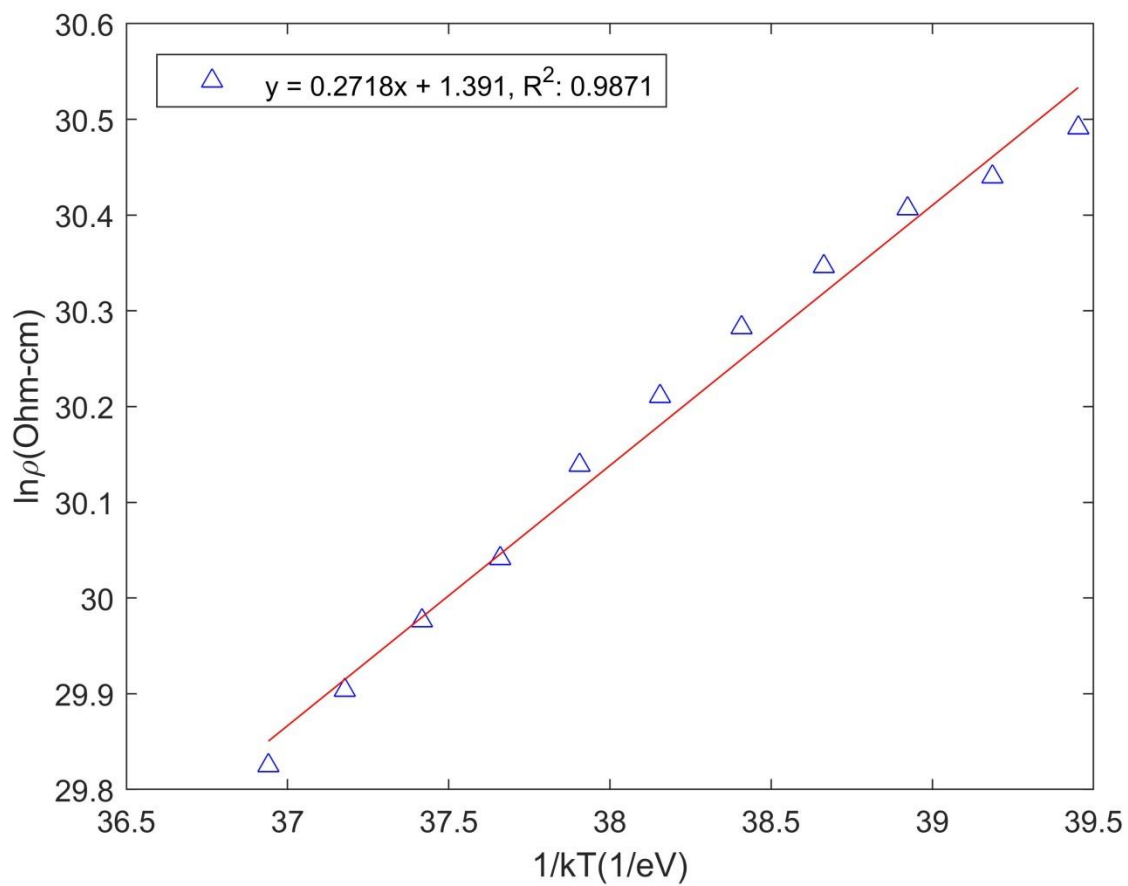


Fig 3.1 Plot of $\ln(\rho)$ vs $1/kT$ for $\text{Ge}_{0.36}\text{Si}_{0.04}\text{Sn}_{0.11}\text{O}_{0.43}$

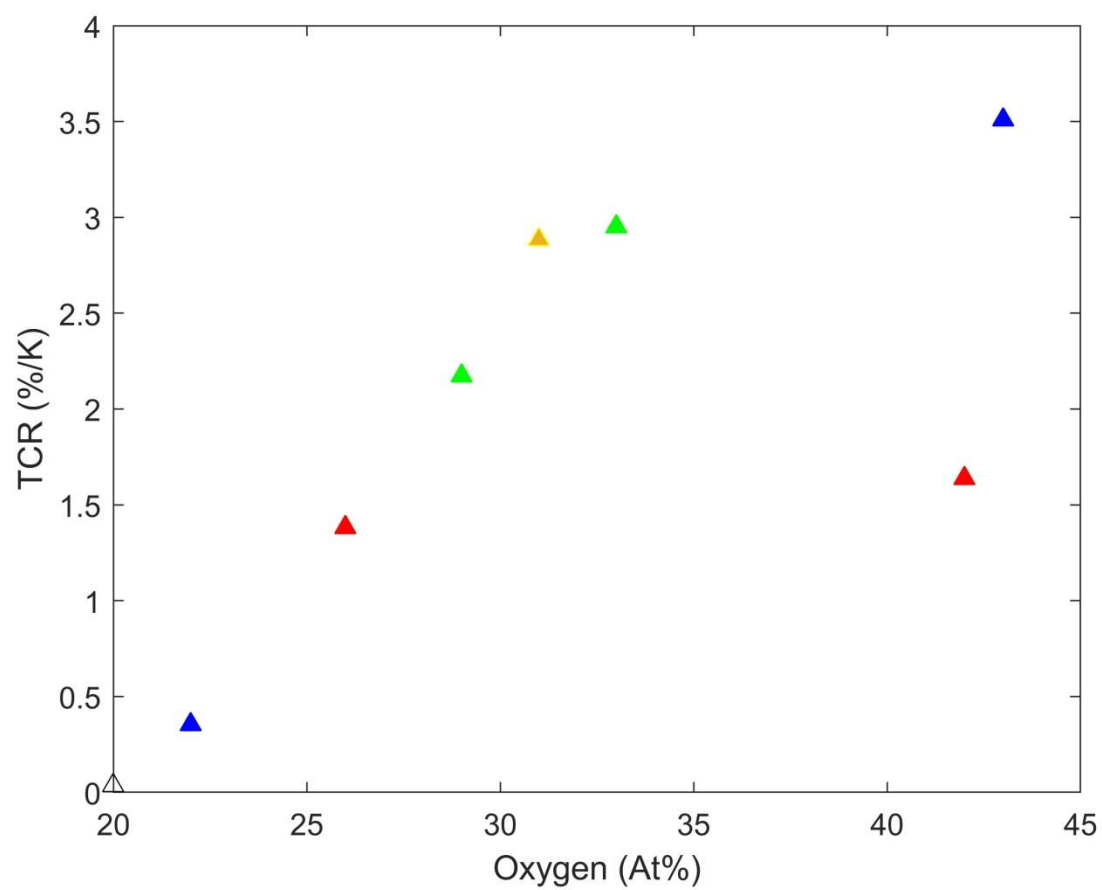


Fig 3.2 Variation of TCR with Oxygen concentration

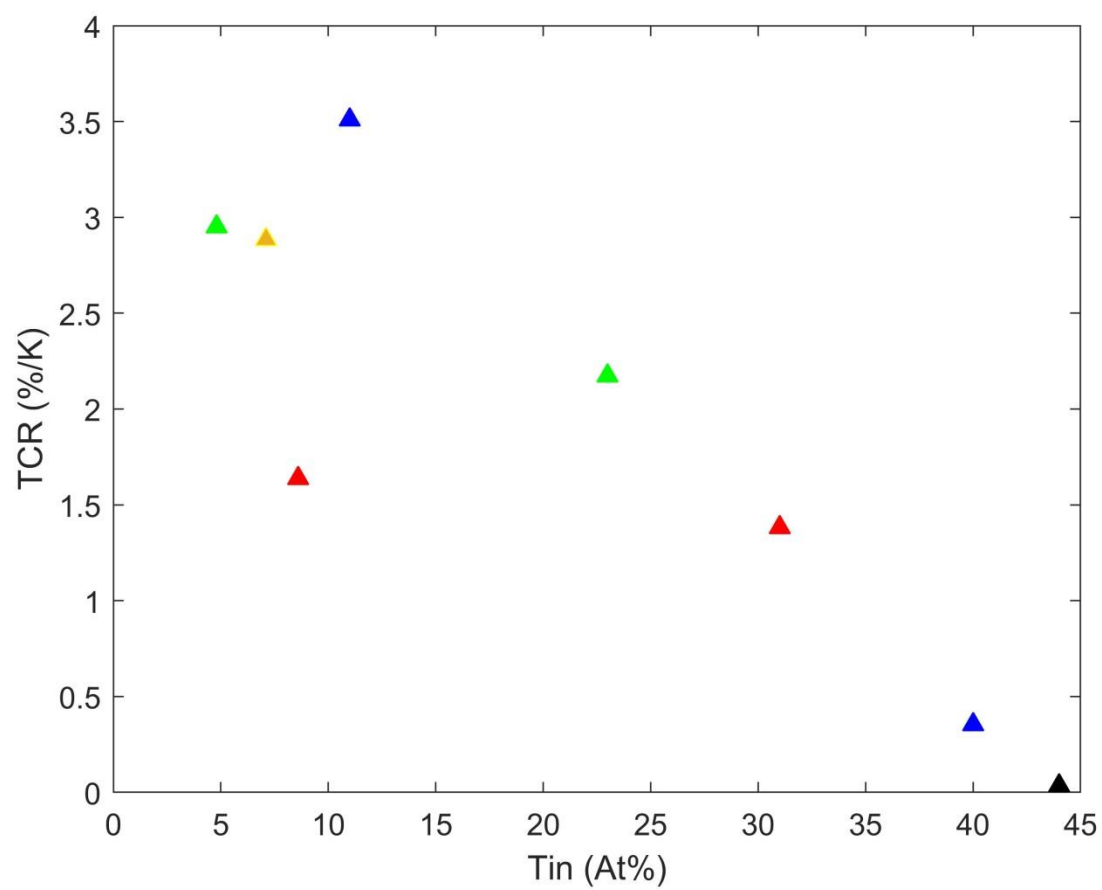


Fig 3.3 Variation of TCR with Tin concentration

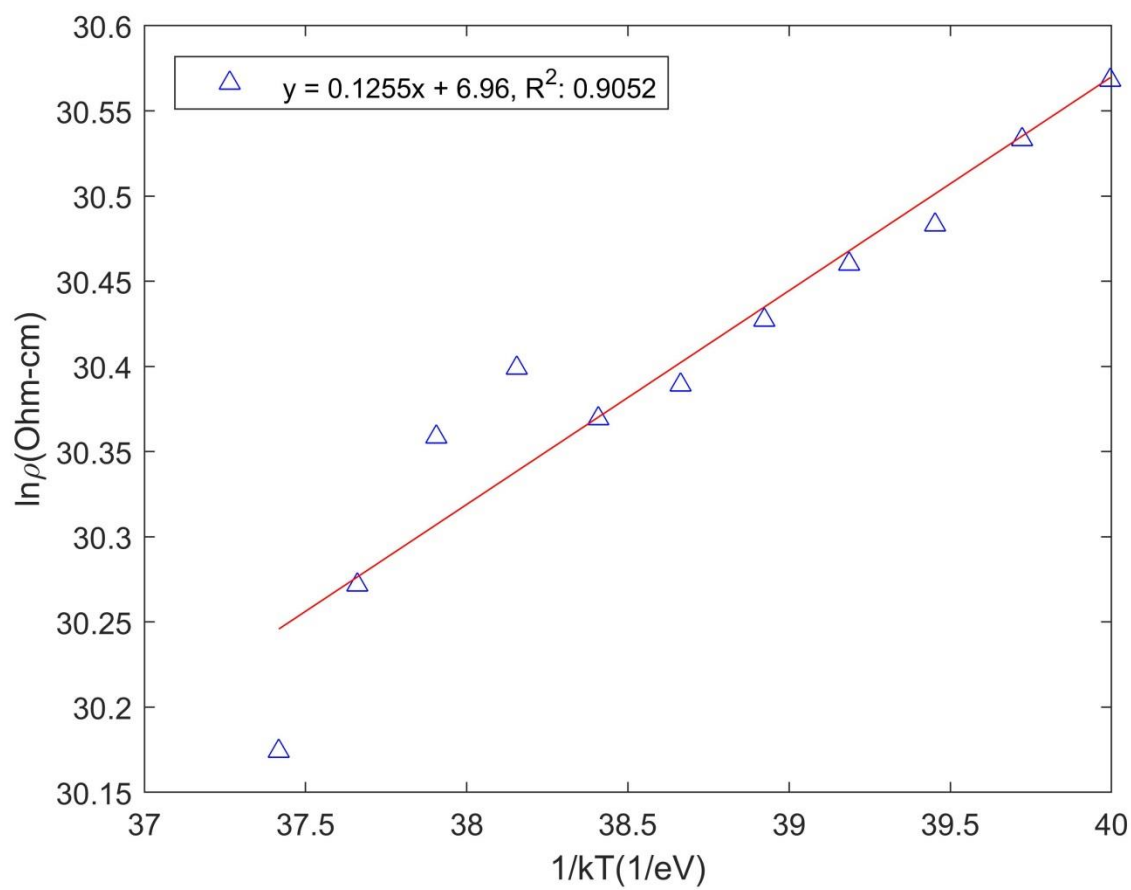


Fig 3.4 Plot $\ln(\rho)$ vs $1/kT$ plot for $\text{Ge}_{0.41}\text{Si}_{0.01}\text{Sn}_{0.09}\text{O}_{0.42}$

low TCR. The reason for adding tin into the thin film alloy is to increase the amount of absorption in the IR region. Fig 3.5, 3.6, and 3.7 shows that the films perform as expected with transmittance/reflectance decreasing and absorption increasing with increasing tin concentration. It is shown that when tin concentration is lower than 30% the transmittance is much higher than when over 30 %, after that the transmittance is not much higher. From Fig 3.5 it can be seen that reflectance is relatively similar for all cases, except for when the tin concentration is over 40 % then as with transmittance there is no reflection. At tin concentrations over 40 % all IR radiation is absorbed.

From the transmittance and reflectance the absorption coefficient (α) can be determined. The absorption coefficient is the value that describes how different wavelengths of light pass through a material before it is absorbed. A small absorption coefficient would mean that the material is transparent to the light. Absorption coefficient is determined by:

$$T = \frac{(1 - r)^2 \exp(-\alpha x)}{1 - r^2 \exp(-2\alpha x)} \quad (3.2)$$

Where T is transmittance, r is reflectance, and x is film thickness. The optical band gap is the cut off frequency of the sensing material. Only light that has a greater energy than the optical band gap energy can be absorbed. Light with lower energy than the band gap will pass through the material, as if it were transparent. The optical band gap, E_g , was determined by fitting the absorption coefficient, α , to Tauc's [19-22] relation for semiconductors.

$$(\alpha h\nu)^{\frac{1}{n}} = B(h\nu - E_g) \quad (3.3)$$

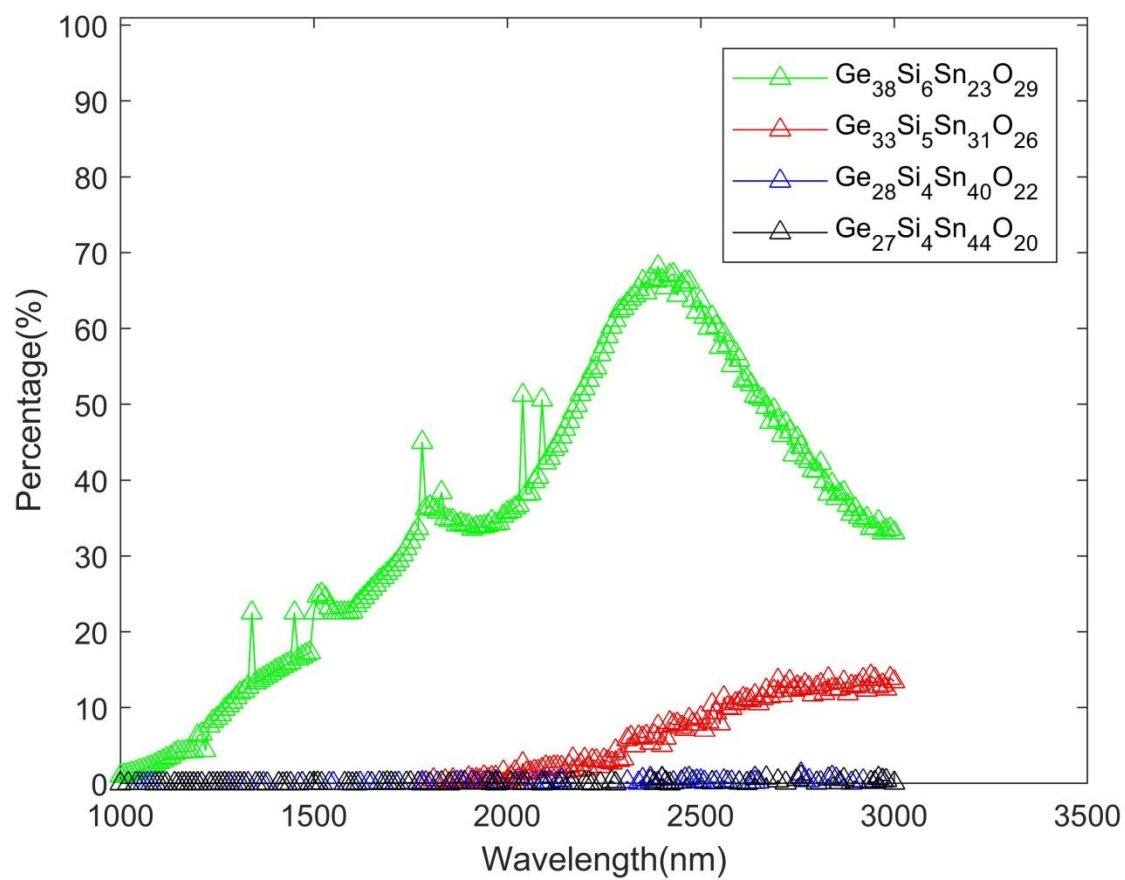


Fig 3.5 Transmittance of four different GeSiSnO thin films

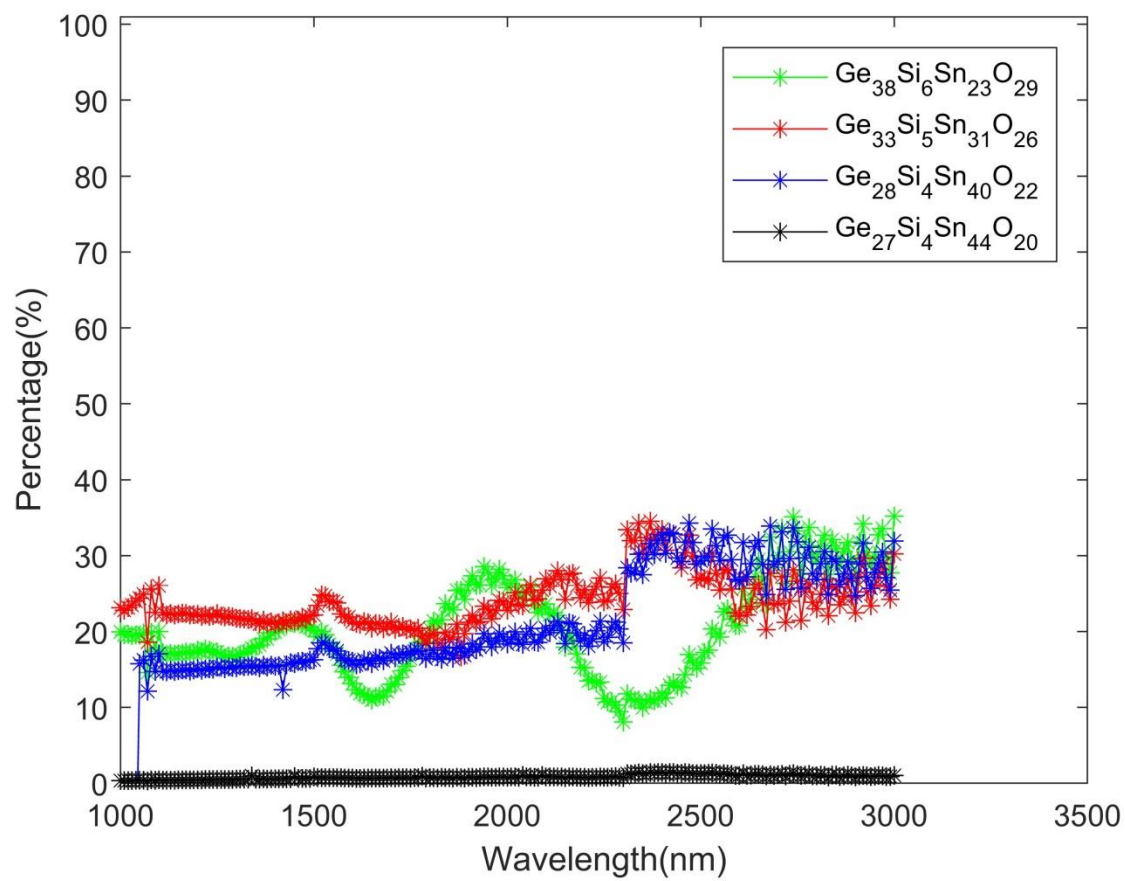


Fig 3.6 Reflectance of four different GeSiSnO thin films

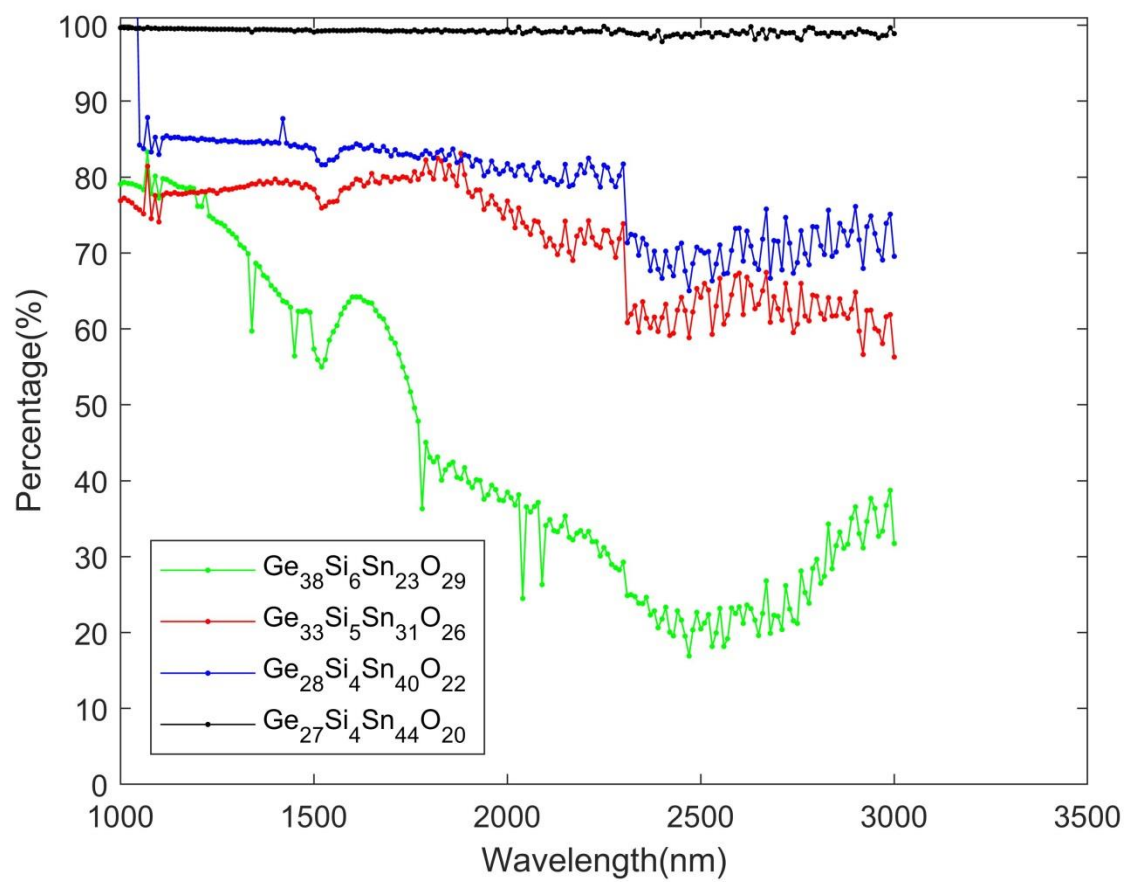


Fig 3.7 Absorption of four different GeSiSnO thin films

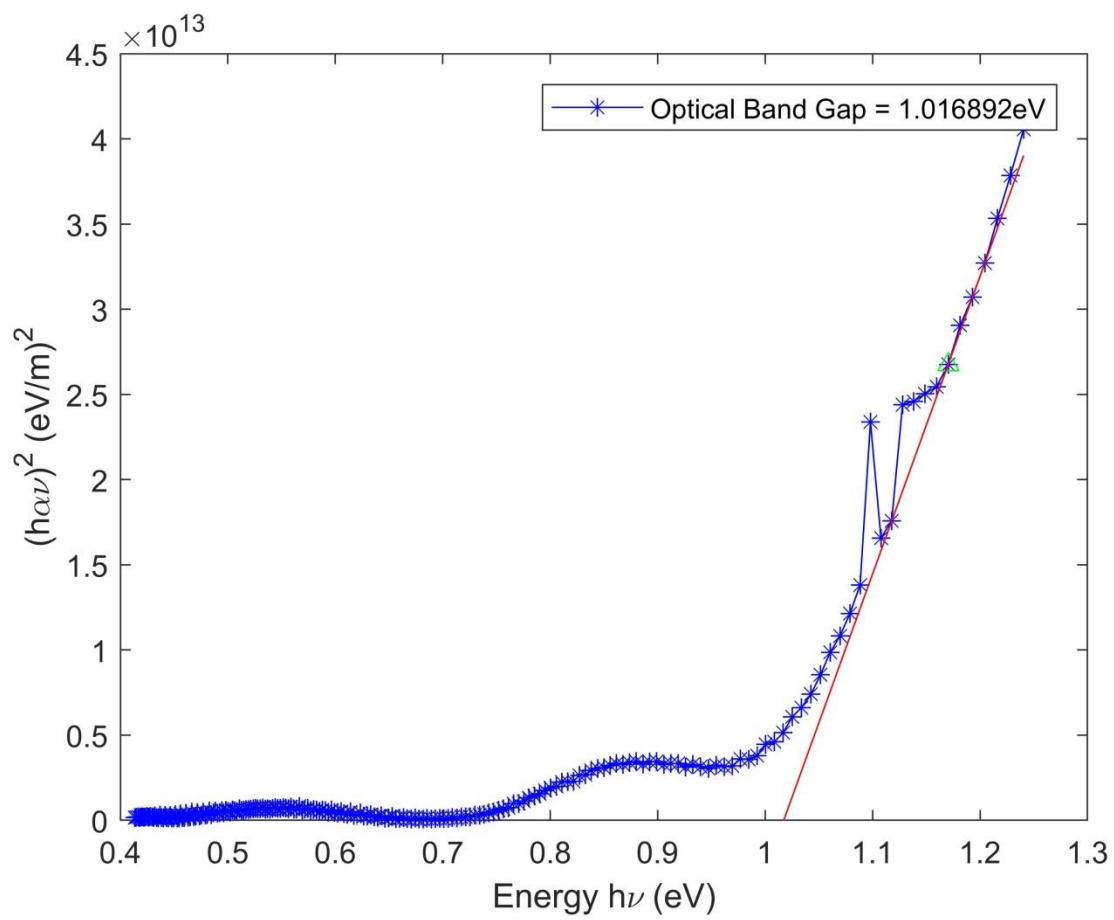


Fig 3.8 Optical band gap plot for GeSiSnO

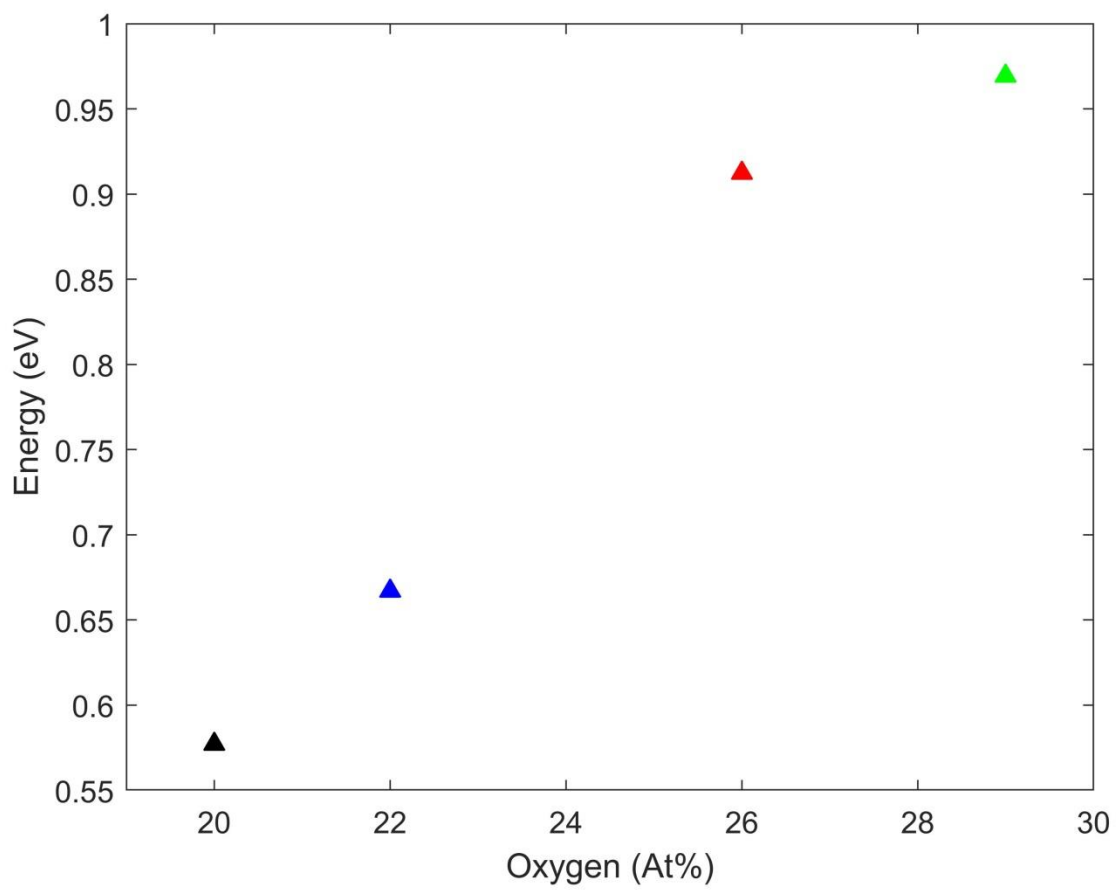


Fig 3.9 Variation of Optical band gap and Oxygen concentration

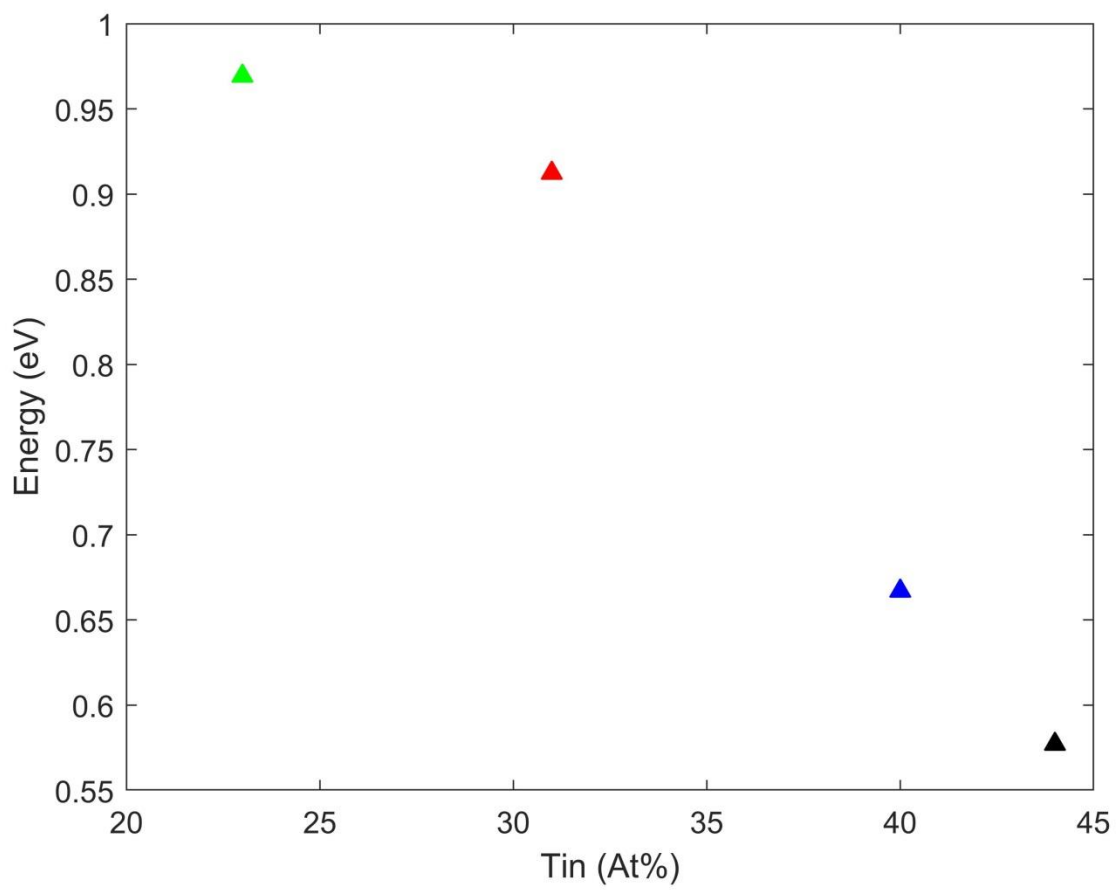


Fig 3.10 Variation of the Optical band gap and the Tin concentration

Where, ν is the frequency, B is a constant, and n can be $\frac{1}{2}$ or 2 depending on whether the material is a direct or indirect semiconductor. The band gap of a semiconductor is the distance between the conduction and valence band measured in eV. It is the energy required to promote an electron from the top of the valence band to the bottom of the conduction band. The energy in our case refers to the energy from a photon. This is needed in order to have current flow. A band gap can be direct or indirect. The conduction and valence band both have their own crystal momentum (k -vector). If the k vector is the same for the top of the valence band/bottom of the conduction band then the film is a direct band gap semiconductor. If they are not the same then the film is an indirect band gap semiconductor. In order to determine whether $\text{Ge}_x\text{Si}_y\text{Sn}_z\text{O}_{1-x-y-z}$ is direct or indirect the optical band gap plot Fig 3.8 had to be plotted with $n = \frac{1}{2}$ and 2 . Whichever plot produced a plot that had a linear region then that was the plot of the optical band gap and therefore determined that the film is direct or indirect. $\text{Ge}_x\text{Si}_y\text{Sn}_z\text{O}_{1-x-y-z}$ was found to be a direct semiconductor, so n is equal to $\frac{1}{2}$. In Fig 3.8, it can be seen that the optical band gap is found by finding the linear region of the $(h\nu)^2$ vs the photon energy ($h\nu$) [19-22]. Fig 3.9 and 3.10 show the variation in band gap energy oxygen/tin concentration. From these plots it can be determined that a higher tin concentration leads to a lower band gap energy and vice-versa for oxygen concentration vs band gap energy. This is as expected since it was already determined that greater tin concentration leads to greater absorption.

Below is a table that compares the results of $\text{Ge}_{0.36}\text{Si}_{0.04}\text{Sn}_{0.11}\text{O}_{0.43}$ with other well-known sensing layer materials.

Table 3.1: Comparison of Different Sensing Layer Materials

	Resistivity, ρ (Ω -cm)	Activation Energy (eV)	TCR (%/K)	References
$\text{Ge}_{0.36}\text{Si}_{0.04}\text{Sn}_{0.11}\text{O}_{0.43}$	1.885×10^5	0.2718	-3.66	Current work
V_2O_5	1.7	0.214	-2.8	Kumar et al [13]
a-SiGe	40	0.1532	-2	Yon et al [14]
poly-SiGe	N/A	0.1463	-1.91	Dong et al [23]
poly-SiGe(CVD deposited)	N/A	0.1532	-2	Sedky et al [24]
a-Si:H	N/A	0.214-0.2987	-2.8 to -3.9	Sylliaos et al [25]
a-Si:H(sandwich)	N/A	0.3447	-4.5	Unewisse et al [26]
a- $\text{Ge}_x\text{Si}_{1-x}\text{O}_y$	2.45×10^2 - 3.34×10^2	0.3723 and 0.4925	-4.86 and -6.43	Cheng et al [12]
$\text{V}_{0.95}\text{W}_{0.05}$	40	0.3141	-4.1	Han et al

				[27]
--	--	--	--	------

CHAPTER 4: DISCUSSION AND CONCLUSION


The results of the characterization results show that $\text{Ge}_x\text{Si}_y\text{Sn}_z\text{O}_{1-x-y-z}$ is an alloy that depends greatly on the amount of tin that is present. When large amounts of tin are present the film will absorb IR radiation to a greater degree than when there is small amounts of tin present. This follows the initial hypothesis that was presented for why tin should be added to the known semiconducting thin film material $\text{Ge}_x\text{Si}_{1-x}\text{O}_y$. The down side being that the TCR of the film goes in the opposite direction. Greater tin concentration leads to a lower TCR. Thus there is a balancing act that has to be maintained in order to have a viable alloy. There was also the unforeseen change in the films semiconducting behavior when oxygen concentration exceeded 40 % and tin concentration fell below 10 %. More investigation on why the alloy begins to act in the opposite manner of a semiconductor when oxygen is greater than 40 % and tin is less than 10 % is needed. If this issue can be resolved then an even greater TCR value may be possible, further increasing the viability of $\text{Ge}_x\text{Si}_y\text{Sn}_z\text{O}_{1-x-y-z}$ as a sensing layer material.

$\text{Ge}_x\text{Si}_y\text{Sn}_z\text{O}_{1-x-y-z}$ thin films were developed through RF and DC magnetron sputtering. The electrical and optical properties were tested, and a GeSiSnO that had a TCR greater than -3.5 %/K and moderate band gap energy (~ 1 eV) was found to exist in $\text{Ge}_{0.36}\text{Si}_{0.04}\text{Sn}_{0.11}\text{O}_{0.43}$. As TCR is the most valuable aspect of the sensing layer in a microbolometer it was important to find a composition that could produce a TCR greater than the current most used sensing layer materials of vanadium oxide and amorphous silicon. The band gap value does limit this composition for use in the NIR because any light with greater wavelength value won't be absorbed. Though there were other compositions whose bandgap values made allowed for use in larger wavelength regions of IR; as long as the sacrifice in TCR was made. As can be seen in Table 3.1 the $\text{Ge}_{0.36}\text{Si}_{0.04}\text{Sn}_{0.11}\text{O}_{0.43}$ alloy is either on par with current standards or slightly beats out the

average standard values. The noise will also be a problem to overcome as $\text{Ge}_{0.36}\text{Si}_{0.04}\text{Sn}_{0.11}\text{O}_{0.43}$ value was found to be $300 \mu\text{V}/\sqrt{\text{Hz}}$ at 10Hz using the system shown in Fig 2.9. Though lowering this value should be possible through forming gas passivation as shown by Rana et. al. [28]. Besides a high noise value $\text{Ge}_x\text{Si}_y\text{Sn}_z\text{O}_{1-x-y-z}$ has been shown to have the necessary characteristics for use in a microbolometer sensing layer. Therefore, the next step would be to fully develop the microbolometer for real world use. From there the complete figures of merit can be tested with $\text{Ge}_x\text{Si}_y\text{Sn}_z\text{O}_{1-x-y-z}$ as the sensing layer material. Based on this work, the author had been approved a patent recently (US patent number 10337927) with Mukti Rana as seen in the Appendix A [29].

Appendix A

Patent Approval Notice for Patent No. 10337927

UNITED STATES PATENT AND TRADEMARK OFFICE				
				
UNITED STATES DEPARTMENT OF COMMERCE United States Patent and Trademark Office Address: COMMISSIONER FOR PATENTS P.O. Box 1450 Alexandria, Virginia 22313-1450 www.uspto.gov				
APPLICATION NO.	ISSUE DATE	PATENT NO.	ATTORNEY DOCKET NO.	CONFIRMATION NO.
16/127,589	07/02/2019	10337927		5095
	7590	06/12/2019		
MUKTI RANA				

ISSUE NOTIFICATION

The projected patent number and issue date are specified above.

Determination of Patent Term Adjustment under 35 U.S.C. 154 (b)
(application filed on or after May 29, 2000)

The Patent Term Adjustment is 0 day(s). Any patent to issue from the above-identified application will include an indication of the adjustment on the front page.

If a Continued Prosecution Application (CPA) was filed in the above-identified application, the filing date that determines Patent Term Adjustment is the filing date of the most recent CPA.

Applicant will be able to obtain more detailed information by accessing the Patent Application Information Retrieval (PAIR) WEB site (<http://pair.uspto.gov>).

Any questions regarding the Patent Term Extension or Adjustment determination should be directed to the Office of Patent Legal Administration at (571)-272-7702. Questions relating to issue and publication fee payments should be directed to the Application Assistance Unit (AAU) of the Office of Data Management (ODM) at (571)-272-4200.

APPLICANT(s) (Please see PAIR WEB site <http://pair.uspto.gov> for additional applicants):

Mukti Rana, Dover, DE;
Jaime Damiany Cardona, Dover, DE;

Appendix B

Constants

Planck's constant, h	$4.135 \times 10^{-15} \text{ eV} \cdot \text{s}$
Boltzmann's constant, k_B	$8.617 \times 10^{-5} \text{ eV/K}$
Speed of light, c	$3 \times 10^8 \text{ m/s}$
Stefan-Boltzmann constant, σ	$5.67 \times 10^{-8} \text{ W/(m}^2 \cdot \text{K}^4)$

REFERENCES

- [1] Planck, M., *The Theory of Heat Radiation*, Dover, New York, 1991.
- [2] Rogalski, A., "Infrared detectors: status and trends," *Progress in Quantum Electronics* vol. 27, pp.59-210, 2003.
- [3] Rogalski, A., "Infrared thermal detectors versus photon detectors: I. Pixel performance," *Material science and material properties for infrared optoelectronics, proceedings*, vol. 3182, pp. 14-25, 1997.
- [4] Kruse, P. W. and Skatrud, D. D., "Uncooled Infrared Imaging Arrays and Systems," *Semiconductors and Semimetals*, vol. 47, pp 17-42, Academic Press, New York, 1997.
- [5] Richards, P. L., "Bolometers for infrared and millimeter waves," *Journal of Applied Physics* 76, 1 (1994).
- [6] Vollmer, M, L. Mollmann, K, P., "Infrared Thermal Imaging Fundamentals, Research, and Applications," Wiley-VCH Verlag GmbH & Co. Weinheim, Germany 2010.
- [7] ASTM Committee F.07 on Nondestructive Testing, "Standard Test Method for Noise Equivalent Temperature Difference of Thermal Imaging Systems," Designation: E1543-00, Reapproved December 2011, Published March 2012.
- [8] North Atlantic Treaty Organization, "Experimental Assessment Parameters and Procedures for Characterization of Advanced Thermal Imagers," RTO Technical Report 75 (II), 2003.
- [9] Rana, M. M., and Butler, D. P., "Radio frequency sputtered Si_{1-x}Ge_x and Si_{1-x}Ge_xO_y thin films for uncooled infrared detectors," *Thin Solid Films*, vol. 514, 2006, pp. 355-360.
- [10] Sedky, S., Fiorini, P., Baert, K., and Mertens, R., "Characterization and optimization of infrared poly SiGe bolometers," *IEEE Transaction of Electron Devices*, vol. 46, no. 4, 1999, pp. 675-682.

- [11] Butler, D. P., Çelik-Butler, Z., and Sobolewski, R., “Yttrium barium copper oxide as an infrared radiation sensing material,” in Handbook of Advanced Electronic and Photonic Material and Devices, Edi. H. S. Nalwa, vol. 3, 2001, pp. 169-195.
- [12] Cheng, Q., Almasri, M., “Silicon germanium oxide ($\text{Si}_x\text{Ge}_{1-x}\text{O}_y$) infrared material for uncooled infrared detection,” Proc. SPIE, 7298, 72980K, 2009.
- [13] Kumar, R.T. Karunagaran, B., Mangalaraj, D., Narayandass, SK., Manoravi, P., Joseph, M., Gopal, V., Madaria, R., and Singh, J.P., “Room temperature deposited vanadium oxide thin films for uncooled infrared detectors”, Materials Research Bulletin 38, 1235-1240, (2003).
- [14] Yon, J., Nieto, J., Vandroux, L., Imperinetti, P., Rolland, E., Goudan, V., Vialle, C., and Arnud A., “Low[resistance a-SiGe-based microbolometer pixel for future smart IR FPA,” Proc., SPIE 7660, Infrared Technology and Applications XXXVI, 76600U (May 03, 2010); doi 10.1117/12.850862
- [15] Iborra, E., Clement, M., Herrero, L. V., Samgrador, J., “IR uncooled bolometers based on amorphous $\text{Ge}_x\text{Si}_{1-x}\text{O}_y$ on silicon micromachined structures,” IEEE/JMEMS, vol. 11, pp. 322-329, 2002.
- [16] “BOROFLOAT®.” *BOROFLOAT® Transmission Curve / Thickness 2mm*, www.pgo-online.com/intl/curves/boro_kurve.html.
- [17] “Sapphire Optical Properties and Sapphire Optical Transmission.” *Valley Design*, www.valleydesign.com/sapppic.htm.
- [18] Optical Materials: Germanium (Ge) a:Visited { Color: #787878; } a:Hover { Color: #971a1e; } a:Active { Color: #971a1e; }, www.iiviinfrared.com/Optical-Materials/ge.html.
- [19] Tauc, J., Grigorovici, R., Vancu, A., “Optical properties and electronic structure of amorphous germanium,” Physics Status Solidi, vol. 15, 1966, pp. 627-637.

- [20] Moharram, A. H., Othman, A. A., Osman, M. A., “Optical characterization of amorphous Ga₅₀Se₄₅S₅ films,” *Applied Surface Science*, vol. 200, 2002, pp. 143- 149.
- [21] Kavak, H., Eker, S., and Mamedov, A., “Harmonic oscillator model and determination of optical parameters,” *Journal of Quantitative Spectroscopy and Radiative Transfer*, vol. 86, 2004, pp. 223-229.
- [22] Bang, T. H., Choe, S. H., Park, B. N., Jin, M. S., and Kim, W. T. “Optical energy gap of CuAl₂S₄,” *Semiconductor Science and Technology*, vol. 11, 1996, pp. 1159-1162.
- [23] Dong, L., Yue, R., and Liu, L. “An uncooled microbolometer infrared detector based on Poly-SiGe thermistier”, *Sensors and Actuators, A* 105, 286-92, (2003).
- [24] Sedky, S., Fiorini, P., Caymax, M., Verbist, A., and Baert, C., “IR bolometers made of polycrystalline silicon germanium”, *Sens. Actuators, A* 66, 193-199, (1998).
- [25] Syllaos, A. J., Schimert, T. R., Gooch, R. W., and McCardel, W. L., “Amorphous Silicon Microbolometer Technology”, DOI:<https://doi.org/10.1557/PROC-609-A14.4>.
- [26] Unewisse, M. H., Craig, B. I., and Watson, R. J. et. al., “The growth and properties of semiconductor bolometers for infrared detection,” *Proceedings of SPIE* 2554, 43 (1995).
- [27] Han, Y-H., Kim, K-T., and Moon, S., “ Enhanced characteristics of an uncooled microbolometer using vanadium-tungsten oxide as a thermometric material”, *Applied Physics Letters* 86, 254101-3, (2005).
- [28] Rana, M. M. and Butler, D. P., “Noise Behavior of Si_{1-x}Ge_xO_y Bolometer and its Reduction by Forming Gas Passivation”, *Thin Solid Films*, vol. 516, issue 18, July, 2008, Pages 6499–6503.
- [29] Rana, M. M., Cardona, J. D., “Germanium Tin Oxide Thin Films for Uncooled Infrared Detectors,” Patent No: 10337927, 2019.

